

## Carbon, nitrogen, oxygen and sulfide budgets in the Black Sea: A biogeochemical model of the whole water column coupling the oxic and anoxic parts

M. Grégoire<sup>a,\*</sup>, K. Soetaert<sup>b</sup>

<sup>a</sup> MARE Interfaculty Center for Marine Research, University of Liège, Dep. Oceanology, Sart-Tilman B6c, Allée de la Chimie 3, B-4000 Liège, Belgium

<sup>b</sup> Netherlands Institute of Ecology, Center for Estuarine and Marine Ecology, P.O. Box 140, 4400 AC Yerseke, The Netherlands

### ARTICLE INFO

#### Article history:

Received 24 April 2009

Received in revised form 2 June 2010

Accepted 5 June 2010

Available online 6 July 2010

#### Keywords:

Biogeochemical cycles

Anoxic waters

Mathematical model

Black Sea

### ABSTRACT

Carbon, nitrogen, oxygen and sulfide budgets are derived for the Black Sea water column from a coupled physical–biogeochemical model. The model is applied in the deep part of the sea and simulates processes over the whole water column including the anoxic layer that extends from  $\approx 115$  m to the bottom ( $\approx 2000$  m). The biogeochemical model involves a refined representation of the Black Sea foodweb from bacteria to gelatinous carnivores. It includes notably a series of biogeochemical processes typical for oxygen deficient conditions with, for instance, bacterial respiration using different types of oxidants (i.e. denitrification, sulfate reduction), the lower efficiency of detritus degradation, the ANAMMOX (ANAerobic AMMONium OXidation) process and the occurrence of particular redox reactions. The model has been calibrated and validated against all available data gathered in the Black Sea TU Ocean Base and this exercise is described in Grégoire et al. (2008). In the present paper, we focus on the biogeochemical flows produced by the model and we compare model estimations with the measurements performed during the R.V. KNORR expedition conducted in the Black Sea from April to July 1988 (Murray and the Black Sea Knorr Expedition, 1991). Model estimations of hydrogen sulfide oxidation, metal sulfide precipitation, hydrogen sulfide formation in the sediments and water column, export flux to the anoxic layer and to the sediments, denitrification, primary and bacterial production are in the range of field observations.

With a simulated Gross Primary Production (GPP) of  $7.9 \text{ mol C m}^{-2} \text{ year}^{-1}$  and a Community Respiration (CR) of  $6.3 \text{ mol C m}^{-2} \text{ year}^{-1}$ , the system is net autotrophic with a Net Community Production (NCP) of  $1.6 \text{ mol C m}^{-2} \text{ year}^{-1}$ . This NCP corresponds to 20% of the GPP and is exported to the anoxic layer. In order to model Particulate Organic Matter (POM) fluxes to the bottom and hydrogen sulfide profiles in agreement with in situ observations, we have to consider that the degradation of POM in anoxic conditions is less efficient than in oxygenated waters as it has often been observed (see discussion in Hedges et al., 1999). The vertical POM profile produced by the model can be fitted to the classic power function describing the oceanic carbon rate ( $C_R = Z^{-\alpha}$ ) using an attenuation coefficient  $\alpha$  of 0.36 which is the value proposed for another anoxic environment (i.e. the Mexico Margin) by Devol and Hartnett (2001). Due to the lower efficiency of detritus degradation in anoxic conditions and to the aggregation of particles that enhanced the sinking, an important part of the export to the anoxic layer (i.e. 33%,  $0.52 \text{ mol C m}^{-2} \text{ year}^{-1}$ ) escapes remineralization in the water column and reaches the sediments. Therefore, sediments are active sites of sulfide production contributing to 26% of the total sulfide production.

In the upper layer, the oxygen dynamics is mainly governed by photosynthesis and respiration processes as well as by air–sea exchanges.  $\approx 71\%$  of the oxygen produced by phytoplankton (photosynthesis+nitrate reduction) is lost through respiration,  $\approx 21\%$  by outgassing to the atmosphere,  $\approx 5\%$  through nitrification and only  $\approx 2\%$  in the oxidation of reduced components (e.g.  $\text{Mn}^{2+}$ ,  $\text{Fe}^{2+}$ ,  $\text{H}_2\text{S}$ ).

The model estimates the amount of nitrogen lost through denitrification at  $307 \text{ mmol N m}^{-2} \text{ year}^{-1}$  that can be partitioned into a loss of  $\approx 55\%$  through the use of nitrate for the oxidation of detritus in low oxygen conditions,  $\approx 40\%$  in the ANAMMOX process and the remaining  $\approx 5\%$  in the oxidation of reduced substances by nitrate.

In agreement with data analysis performed on long time series collected since the 1960s (Konovalov and Murray, 2001), the sulfide and nitrogen budgets established for the anoxic layer are not balanced in response to the enhanced particle fluxes induced by eutrophication: the  $\text{NH}_4$  and  $\text{H}_2\text{S}$  concentrations increase.

© 2010 Elsevier B.V. All rights reserved.

\* Corresponding author. Tel.: +32 43663354.

E-mail address: [mgregoire@ulg.ac.be](mailto:mgregoire@ulg.ac.be) (M. Grégoire).

## 1. Introduction

### 1.1. Vertical thermohaline structure

The Black Sea is a land locked basin (Fig. 1), permanently stratified by the inflow of large river runoffs at the surface and the incursion at depth ( $\approx 500$  m) of saline Mediterranean water through the Bosphorus Strait. Differently from what is known about the open ocean, due to this permanent halocline, only the first 100–150 m of the water column are influenced by atmospheric fluxes and present a pronounced seasonal variability. Therefore, surface waters are decoupled from the deep waters and the vertical circulation is more than ten times less intense than the integrated horizontal circulation (Stanev, 1990). The only transport registered in the deep waters is associated with convective motions driven by geothermal heat fluxes leading to the formation of a bottom convection layer which is the largest (400–500 m) ever observed in the world ocean (Top et al., 1991). Also, waters below 500 m depth are essentially stagnant and the residence time increases from a few years for the layer of the main pycnocline (e.g. Unluata et al., 1990; Buesseler et al., 1991) to several hundred years for the deepest layer (e.g. Murray et al., 1991).

The Black Sea has a positive water balance, in which the inputs from freshwater sources exceed losses by evaporation. Although there is a large variation in the estimates reported, current estimates, based on a review of literature can be given as  $\approx 300 \text{ km}^3 \text{ year}^{-1}$  for precipitation,  $\approx 350 \text{ km}^3 \text{ year}^{-1}$  for runoff waters,  $\approx 350 \text{ km}^3 \text{ year}^{-1}$  for evaporation from the sea surface. The net flux through the Bosphorus accounts for the remaining component of the water budget (Ozsoy and Unluata, 1997). Fig. 2 illustrates the typical annual averaged vertical profiles of salinity, temperature and density for the central basin. Salinity varies from  $\approx 18.2$  at the surface to  $\approx 21.8$  at 300 m. The salinity profile presents a permanent gradient and its structure is governed at the surface by river input and secondary by precipitation/evaporation while, at depths, the intrusion of salty Mediterranean waters increases the salinity. The averaged temperatures range from  $\approx 18.8$  at the surface to  $\approx 8.8$  at 300 m. Seasonally, surface temperatures in the deep sea vary from 6.5 to 7 °C in February–March to 25 °C in August. A permanent Cold Intermediate Layer (CIL) characterized by temperature below 8 °C is located at a depth spatially varying between 30 and 100 m. This layer forms in winter when atmospheric temperatures are well below 8 °C and is thus, well oxygenated. At depth the temperature values are influenced by the penetration of warmer Mediterranean waters.

### 1.2. Vertical biogeochemical structure and eutrophication

Due to the poor ventilation mechanism, oxygen is only contained in the upper 100 m depth and a completely anoxic layer with huge contents of  $\text{H}_2\text{S}$  and  $\text{NH}_4$  constitutes 87% of the sea volume (Fig. 3). This makes the Black Sea an almost completely anoxic basin. At the transition between the oxic and sulfidic layers, a well-developed suboxic zone, characterized by many intermediate redox reactions has been identified (e.g. Murray et al., 1989, 1995). This suboxic layer is characterized by very low concentrations of  $\text{O}_2$  and  $\text{H}_2\text{S}$  ( $\text{O}_2 < 10 \mu\text{M}$  and  $\text{H}_2\text{S} < 5 \text{ nM}$ ), with no overlap between these two quantities (Murray et al., 1995). Its presence implies that direct reaction between oxygen and sulfide does not occur but rather the sulfide diffusing upward from the anoxic layer is oxidized by the lateral injection of oxygen contained in the Mediterranean plume (Konovalov et al., 2003). The remineralization of organic matter by bacteria in the different vertical layers constituting the water column occurs with different types of oxidants: oxygen in the upper oxygenated layer, nitrate in the suboxic layer (i.e. denitrification)

and other oxidants (e.g. manganese oxides, iron oxides, sulphate) in the anoxic layer (see Fig. 3).

Due to its landlocked character, the Black Sea is particularly sensitive to anthropogenic pressures and natural variability. In the 1970s–1980s period, the Black Sea has been submitted to various anthropogenic pressures: eutrophication, dams construction, overfishing and introduction of alien species. These pressures have altered the ecosystem functioning and the distribution of chemical constituents (e.g. Codispoti et al., 1991; Mee, 1992; Tugrul et al., 1992; Niermann et al., 1994; Cociasu et al., 1997; Humborg et al., 1997; Kovalev and Piontkovski, 1998; Kideys et al., 2000; Konovalov and Murray, 2001). For instance, Fig. 3 illustrates the vertical profiles of nitrate, ammonium, oxygen and sulfide before and during eutrophication. The analysis of these data have shown that the increase of nitrate is explained by the increased input from the rivers (mainly the Danube). The increase of primary production induced by eutrophication enhanced the consumption of oxygen in the upper layer and the export of detritus to the deep anoxic layer increasing its ammonium and sulfide content (Konovalov and Murray, 2001).

### 1.3. Objectives of the study presented in this paper

During these last two decades, mathematical biogeochemical models of different complexities have been applied in the Black Sea in order to understand the functioning of its ecosystem. For instance, simple 5 state variables Fasham-like models have been implemented in a 1D (along the vertical coordinate) frame (e.g. Oguz et al., 1996; Staneva et al., 1998) and at basin scale (Grégoire and Lacroix, 2003; Grégoire and Friedrich, 2004; Grégoire et al., 2004). More complex vertically resolved ecological models involving several phytoplankton and zooplankton compartments (e.g. Oguz et al., 2001) as well as an explicit representation of gelatinous groups (Lebedeva and Shushkina, 1994; Lancelot et al., 2002) have been developed in order to simulate the seasonal cycle of the planktonic ecosystem. Some models have been developed in order to study the dynamics of the suboxic layer. For instance, Oguz et al. (2000) extended their ecological models by adding a description of redox reactions of the suboxic layer involving dissolved and particulate manganese as well as hydrogen sulfide. Yakushev and Neretin (1997) and Yakushev et al. (2007) developed a simplified vertically resolved chemical model of the suboxic area involving a refined representation of nitrogen and sulfur compounds. In order to investigate the redox budget of the Black Sea and the impact of climate variability and eutrophication on this budget, Konovalov et al. (2006) elaborated a vertically resolved biogeochemical model of the aphotic zone involving a complete representation of nitrogen, sulfur, manganese and iron cycling.

So far, no model has explicitly simulated biogeochemical processes over the whole water column from the sea surface until the bottom. Most of them are forced by fluxes of chemical constituents ( $\text{H}_2\text{S}$ ,  $\text{NH}_4$ ) at their lower boundary ( $\approx 150$  m) and do not extend down to the bottom. Only the model presented in Konovalov et al. (2006) simulates the whole anoxic layer but this model does not include a representation of the upper layer ecosystem. In this aspect, the present study is innovative because the model simulates the whole water column including the pelagic ecosystem and the whole anoxic layer until the bottom. Processes in the upper oxygenated layer are fully coupled with anaerobic processes in the deep waters allowing to perform long term simulations. The model has been developed in order to understand the modifications of the Black Sea ecosystem due to eutrophication and has been validated using the data collected in the Black Sea TU Ocean Base. The calibration and validation of the model are extensively described in a companion paper (Grégoire et al., 2008). Here, nitrogen, car-

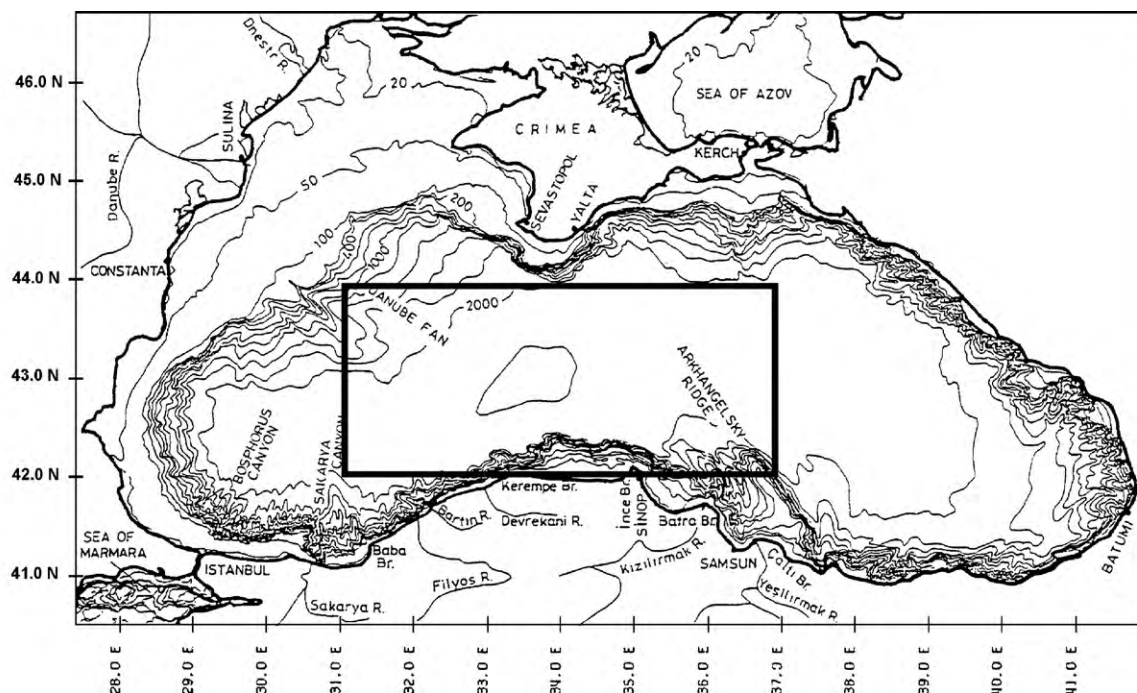


**Fig. 1.** Layout and bathymetry of the Black Sea basin. Depth contours are labeled in meters (figure reproduced from Ozsoy and Unluata, 1997). The north-western part of the basin is occupied by a wide shelf with a mean depth of  $\approx 50$  m. The mid-depth at the shelf break is  $\approx 150$  m. The model is considered to be representative of the situation in the central Black Sea which has been delimited as the region between  $42\text{--}44^\circ\text{N}$ ,  $31\text{--}37^\circ\text{E}$  with a water depth of 2000 m (in the rectangle).

bon, oxygen and sulfide budgets are derived from model results for the oxygenated-suboxic layer and for the anoxic layer. A special focus has been put on the study of biogeochemical processes in the anoxic waters. In particular, we investigate the manner in which the export production is remineralized in the deep anoxic waters and the subsequent attenuation of the export flux through the water column. We determine the main sites of organic matter degradation (water column versus sediments) and subsequent  $\text{H}_2\text{S}$  production. These processes are investigated using conjointly modeling experiments and the conclusions of the KNORR-88 expeditions.

The paper is organized as follows. The data used to initialize, calibrate and validate the coupled model as well as the coupled model structure are described in Section 2. Section 3 presents and discusses model results. More specifically, we discuss the transient adjustment of the model and its convergence to a repeated annual cycle, we present model-derived carbon, nitrogen, oxygen and sulfide budgets. Finally, Section 4 gives a short conclusion.

## 2. Material and methods

### 2.1. Data used for the model calibration/validation

Since the early 1960s until now, many surveys have been organized throughout the basin and have collected physical, chemical and biological data. A large part of these data has been gathered in the Black Sea TU Ocean Base in the frame of NATO projects. This Data Base contains data for 116 variables from 271 data sets, including 8,364,731 data values for 26,035 stations (<http://sfp1.ims.metu.edu.tr/TU-BlackSea/inventory>). These data sets have been described and analyzed in many papers (e.g. for biological data: Shushkina and Vinogradov, 1991; Kovalev and Piontkovski, 1998; Kideys et al., 2000; Yunev et al., 2002, 2005; for chemical data: Codispoti et al., 1991; Tugrul et al., 1992; Saydam et al., 1993; Konovalov and Murray, 2001). The period between 1988 and 1992, which is considered as the most severe eutrophi-

cation phase for the deep sea (Yunev et al., 2002), was well covered with more than 600 chlorophyll *a* measurements in the deep sea ( $>1000$  m). In particular, an expedition consisting of five cruises spread over 4 months of the spring and summer (April 16–July 29) of 1988 were organized on the R.V. Knorr. A special issue of *Deep Sea Research* has been published in 1991 gathering 31 papers that cover the complete range of topics studied during the 1988 expedition (see Murray and the Black Sea Knorr Expedition, 1991). All the data used in the present study were derived from Black Sea TU Ocean Base. We focused our study on the central Black Sea delimited by  $42\text{--}44^\circ\text{N}$ ,  $31\text{--}37^\circ\text{E}$  with a depth of 2000 m (Fig. 1) because data analysis in this area shows that the spatial variability is quite low compared to the temporal variability (seasonal and interannual) (Yunev et al., 2002). More details on the data sets used for the calibration and validation of the model can be found in Grégoire et al. (2008).

### 2.2. Model

The model is applied in the central Black Sea which is more or less isolated from coastal areas and river discharges by the Rim Current. It resolves the whole water column until 2000 m but only along the vertical dimension (1D model). The physical model is the General Ocean Turbulence Model (GOTM) available online at <http://www.gotm.net> and which has been successfully applied in highly contrasting sites ranging from temperate mixed shelf areas to permanently stratified tropical deep-ocean sites (e.g. Blackford et al., 2004; Torres et al., 2006). The biogeochemical model is a coupled carbon–nitrogen–oxygen–silicon model described by 24 state variables. It includes diatoms, dinoflagellates and small phototrophic flagellates (this last group is in fact, an aggregate of pico- and nano-phototrophic flagellates to which belongs coccolithophorids), the micro- and mesozooplankton, the gelatinous omnivores and carnivores zooplankton, bacteria, labile and semi-labile dissolved organic matter, particulate organic matter, oxygen and a lump-sum of reduced substances in the anoxic layer.

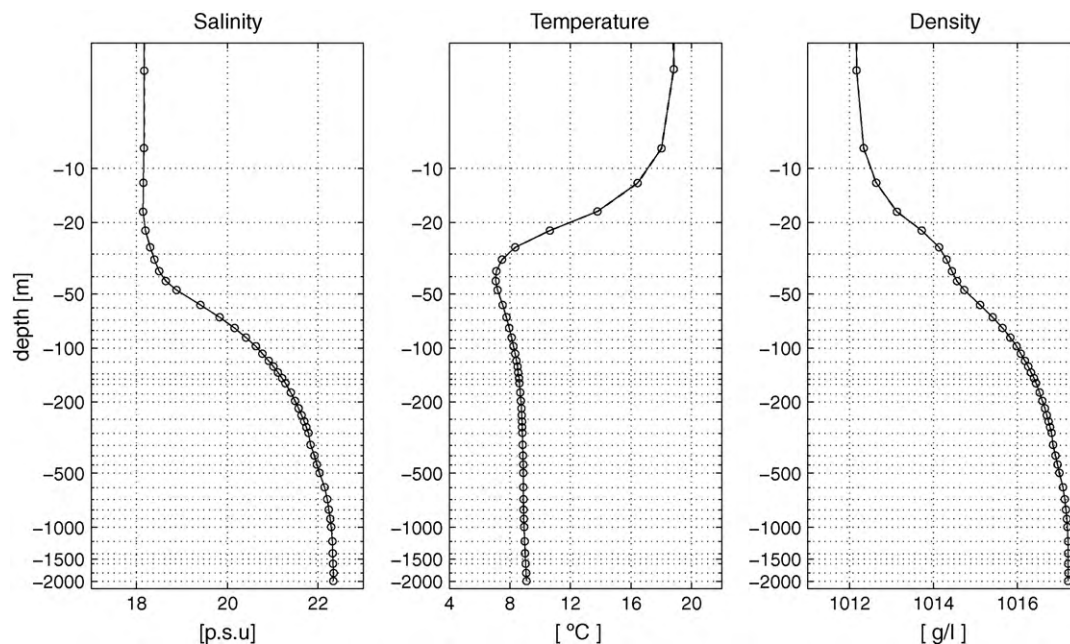


**Fig. 2.** Averaged vertical profiles of salinity, temperature and density computed using all the data ( $\approx 24,000$  data points per profile) available in the area  $42.5\text{--}43.5^\circ\text{N}$ ,  $34\text{--}38^\circ\text{E}$  for the period 1990–2000. The data used are from the Black Sea TU Ocean Base and the MEDAR data base.

The physical and biogeochemical part of the model has been extensively described in [Gregoire et al. \(2008\)](#) as well as the implementation (e.g. initial and boundary conditions, numerical scheme) and calibration procedures. A schematic representation of the ecosystem model showing the interactions between the different compartments is shown in [Fig. 4](#). The model state variables are listed in [Table A.1](#). The state equations of the biogeochemical model are given in [Table A.3](#), and biogeochemical processes are summarized in [Table A.4](#). [Table A.2](#) defines the variables used in [Tables A.3 and A.4](#). The parameters used in these formulations are listed in [Table A.5](#). All Tables and equations are given in [Appendix A](#).

### 3. Results and discussion

#### 3.1. Transient adjustment and convergence to a repeated annual cycle

##### 3.1.1. Transient adjustment

Since we started from realistic initial profiles of temperature and salinity, the physical model reaches a solution which shows a good agreement with temperature, salinity and density observations after one year of integration. However, it should be noted that the non-representation of lateral transport in this 1D model and, in particular, of the Bosphorus Plume, and the absence of a nudg-

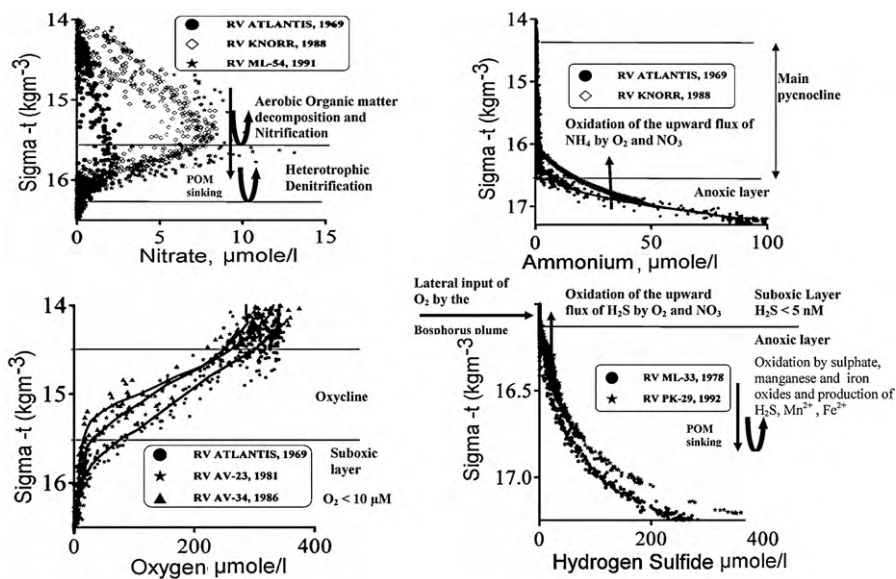


**Fig. 3.** Distributions of nitrate, ammonia, oxygen and hydrogen sulfide ( $\mu\text{mol l}^{-1}$ ) versus  $\sigma_t$  scale for different years (solid line profiles shown for oxygen and ammonia represent an average distribution of oxygen and ammonia derived from individual cruise data sets, data profiles taken from [Tugrul et al. \(1992\)](#) and [Konovalov and Murray \(2001\)](#)). A brief description of important biogeochemical processes (e.g. detritus degradation, redox reactions) has been added. The predominant vertical gradients of biogeochemical properties are confined within the strongly stratified upper 100 m layer, where the density changes by about  $2\text{--}5\text{ kg m}^{-3}$  (from  $\sigma_t \approx 11\text{ kg m}^{-3}$  in summer and  $14\text{--}14.5\sigma_t$  in winter at the surface to  $\sigma_t \approx 16\text{ kg m}^{-3}$  at  $80\text{--}120\text{ m}$  depth) (figure reproduced from [Gregoire et al., 2008](#)).

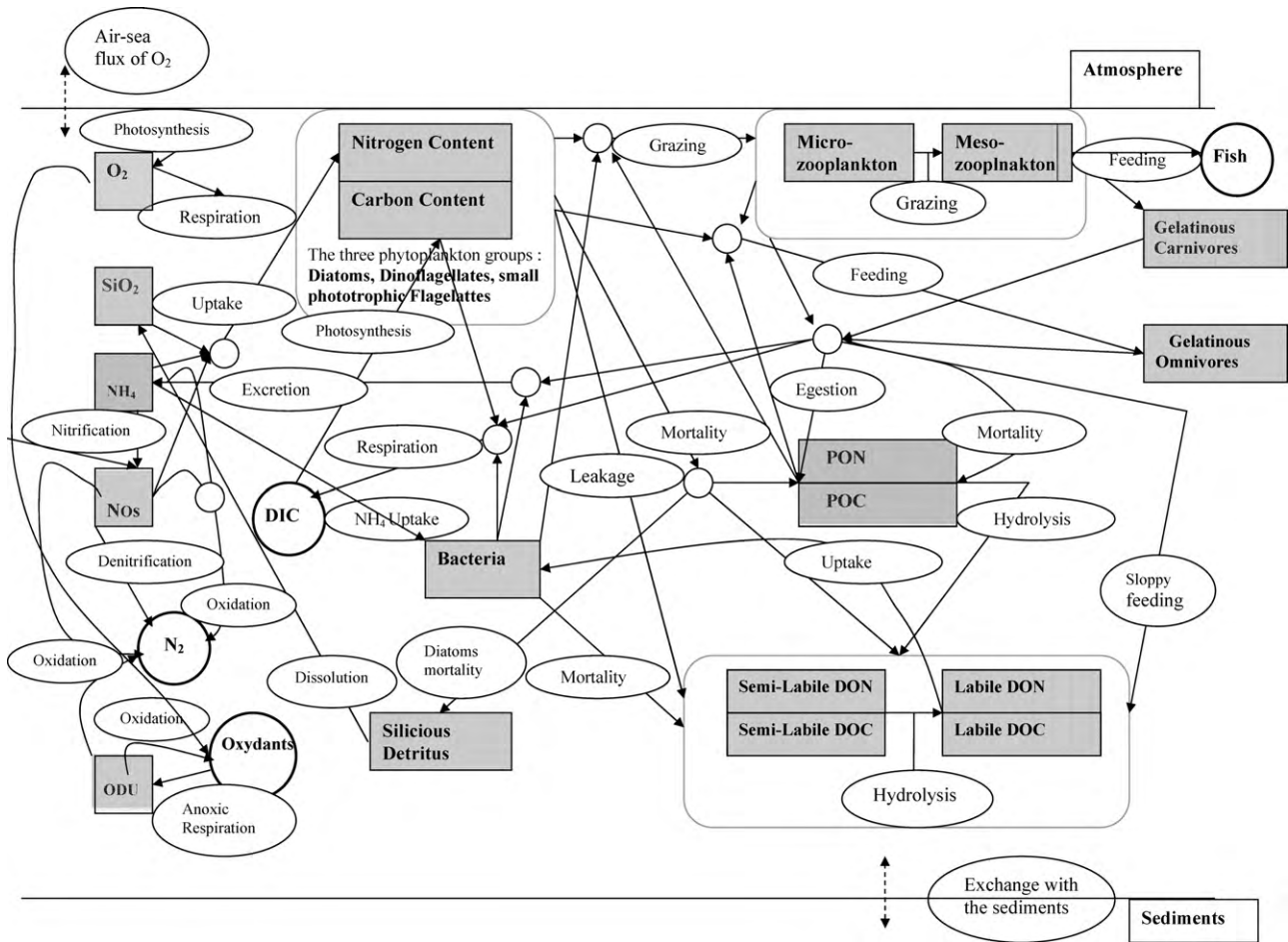


**Fig. 4.** Schematic representation of the ecosystem model. Boxes represent model state variables, arrows represent biogeochemical processes governing the interactions between state variables. Similar processes affecting different state variables are connected by a circle. Boldly encircled variables represent external variables not explicitly modeled (DIC = dissolved inorganic carbon).

ing term lead to the progressive erosion of the halocline and the resulting increased penetration of the vertical mixing.

For the biogeochemical model, the transient adjustment is very long and the convergence of the modelled state variables to a repeated annual cycle needs several years of integration (one or two years of simulation is not long enough). To illustrate this long adjustment, Fig. 5 shows the evolution of the modelled integrated biomass during the first 60 years of integration. This figure shows that model state variables exhibit transient adjustment during the first 30 years of integration. The transient behavior is illustrated by the disappearance and reappearance of some ecological groups. For instance, at the beginning of the simulation, the gelatinous omnivores has an explosive development with biomass reaching 100 mmol C m<sup>-3</sup> at their peak of development in summer. Conversely, at this period, the biomass of gelatinous carnivores is very low. The phytoplankton groups also show important variability during the first years of model integration. Dinoflagellates directly disappear and the phytoplankton blooms are composed of diatoms and small flagellates. After 15 years of model integration, the biomass of the gelatinous omnivores sharply decreases and the gelatinous carnivores become dominant. The enhanced development of the gelatinous carnivores exerts an increasing control on the mesozooplankton development and allows the reappearance of dinoflagellates (Fig. 5). This complex dynamics can be imparted to the explicit representation of the two gelatinous groups. Indeed, these groups have a slower dynamics with growth rates by one to two orders of magnitude lower than those of the micro-

mesozooplankton. It takes a longer time for these groups to reach a steady state and this slow growth has an impact on the lower trophic levels. This long transient period is not present when we do not represent the two gelatinous groups.

The long time of adjustment of the system simulated by the model may be representative of what occurs in the real system after the invasion of the ctenophore *Mnemiopsis*. Indeed, data collected for *Noctiluca* in the deep sea show an increase of biomass up to the 1980s and then a decrease by 1990 of one order of magnitude due probably to the insufficient amount of food conjointly with the explosion of the ctenophore *Mnemiopsis* (Kovalev and Piontkovski, 1998). This is different from what occurs on the north-western shelf where the zooplankton biomass was predominantly composed of *Noctiluca* due probably to the larger amount of food associated to the river discharges and the higher blooms. For the phytoplankton composition, some data collected during the period 1980–1995 in the central basin shows a dominance of dinoflagellates over diatoms during some periods of the year (Mikaelyan, 1997) contrary to the pre-eutrophication period when diatoms was largely dominant.

Finally, we should note that in our simulations we assumed that the upper layer ecosystem is at equilibrium and we run the model until a repeated annual profile is reached. For this reason, we hypothesized that the total nitrogen content of the oxic-suboxic layer is constant and typical of what was observed at the end of the 1980s. To maintain this nitrogen content, we had to compensate for the definitive loss of nitrogen by denitrification and sinking to the

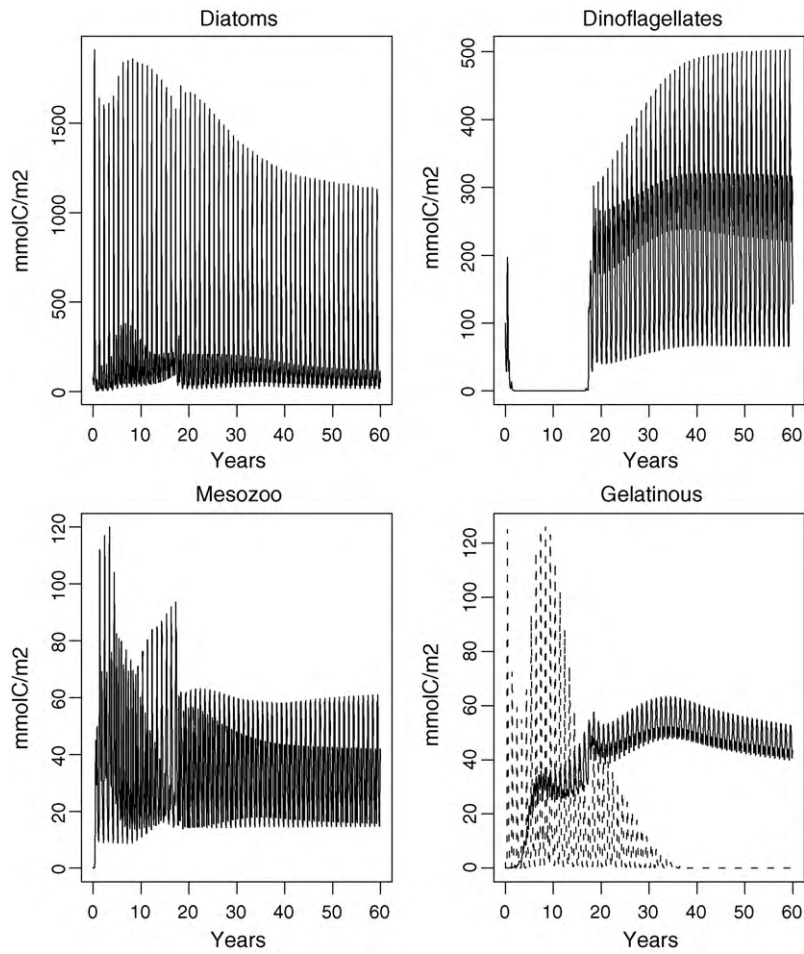


**Fig. 5.** Vertically integrated (in the first 100 m) diatoms, dinoflagellates, mesozooplankton, gelatinous omnivores (in dashed line) and carnivores simulated by the model during the transient adjustment of the model to a repeated annual cycle.

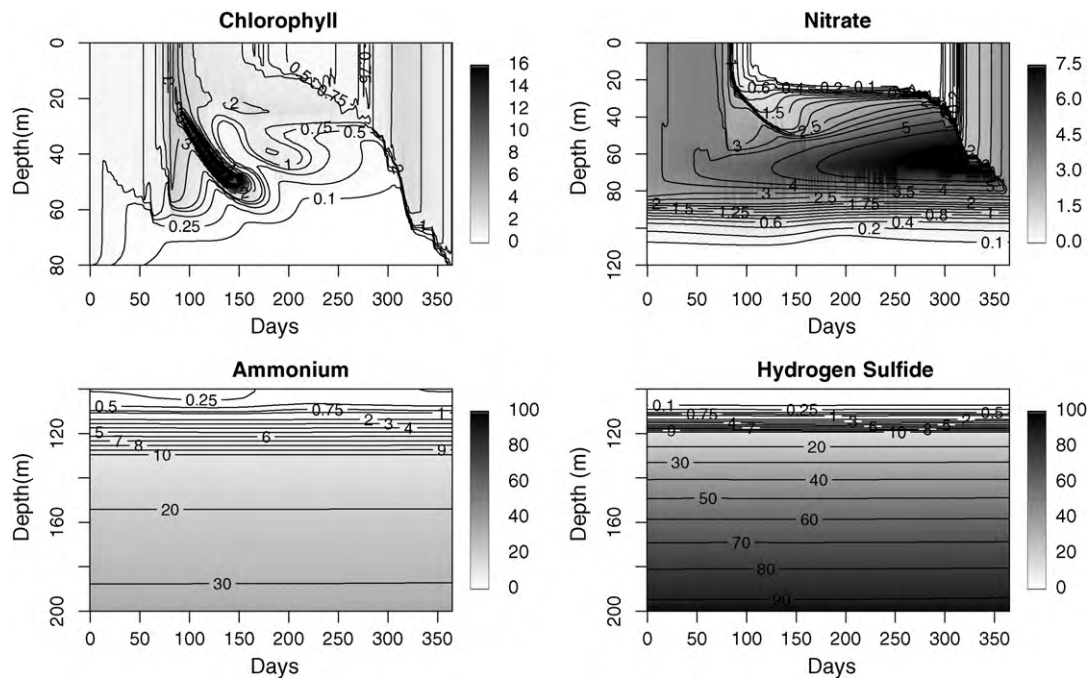


**Fig. 6.** Seasonal evolution of the vertical distribution of chlorophyll (in mg m<sup>-3</sup>), nitrate, ammonium and hydrogen sulfide (deduced from ODU) in mmol m<sup>-3</sup> simulated by the model.

anoxic layer. We impose a lateral nitrogen transport in the form of nitrate into the upper layer mimicking the lateral transport of rich nutrient coastal waters, mainly the Danube. In the same way, we impose a lateral transport of dissolved silicate into the upper layer to compensate for definitive silicate loss associated to the sinking of diatoms and silicious detritus to the anoxic zone.

For the anoxic layer, in order to calibrate the particle dynamics and export, the chemical model was first run off-line with the particle and microbial loop model in order to check its capacity in simulating anoxic waters. After a  $10^4$  year run, the model simulates  $\text{NH}_4$  and  $\text{H}_2\text{S}$  profiles similar to observations. However, the  $\text{NH}_4$  and  $\text{H}_2\text{S}$  contents of the deep waters are found to increase each year of integration suggesting that the Black Sea deep waters are not at equilibrium. These simulations are described in (Grégoire et al., 2008).

### 3.1.2. The converged solution

In the upper layer, the converged solution shows a continuous development of phytoplankton throughout the year (Fig. 6), with an intense spring bloom dominated by diatoms and a fall bloom dominated by dinoflagellates. Dinoflagellates are present throughout the year and dominate from summer until late fall. Model results show periods of silicate limitation in the oxic layer due to the consumption of silicate by blooms of diatoms intensified by the development of gelatinous carnivores. Sensitivity studies have shown that in the absence of gelatinous carnivores the intensity of the diatoms spring bloom is reduced and hence the strong pumping of silicate (silicate was not limiting anymore in the absence of gelatinous carnivores). Therefore, we conclude that the development of dinoflagellates has been favored by the development of gelatinous carnivores due, on the one hand, to the silicate pumping and removal and, on the other hand, by the direct control of gelatinous on mesozooplankton stocks. Small phototrophic flagellates are never dominant in terms of biomass, but are present almost throughout the year except in winter. The omnivorous gelatinous group rapidly extinguishes during the transient phase due to the insufficient prey biomass.

Model results show that the surface layer (0–50 m) is enriched in nitrate from mid-November until late March with maximum concentrations of  $3.8 \text{ mmol N m}^{-3}$  (Fig. 6). Then, nitrate formed by nitrification of regenerated ammonium accumulated at depth with maximum values of  $8.2 \text{ mmol N m}^{-3}$  at 60 m. Below this depth, nitrate concentrations sharply decrease due to denitrification in oxygen deficient waters (see also the oxygen profiles shown in Fig. 11). Ammonium concentrations are very low in the first upper 100 m of the water column due to nitrification process in oxygenated waters. Below, in the absence of oxygen, the ammonium sharply increases due to the degradation of organic matter and the absence of nitrification. Ammonium reaches concentrations of  $\approx 100 \text{ mmol N m}^{-3}$  on the bottom. Hydrogen sulfide exhibits a similar profile with concentration reaching  $\approx 380 \text{ mmol m}^{-3}$  on the bottom. The model is not perfectly successful in the simulation of the suboxic layer. A vertical layer extending from 110 m until 115 m characterized by oxygen and sulfide concentrations lower than  $10 \text{ mmol m}^{-3}$  is simulated. Compared to the informations we have on the suboxic layer (e.g. Murray et al., 1989, 1995), the model underestimates its thickness ( $\approx 30 \text{ m}$  in the observations) and overestimates its sulfide concentrations (which are lower than  $2.5 \times 10^{-3} \text{ mmol m}^{-3}$  in the data). These discrepancies may be partly explained by the absence in the model of lateral injection of oxygen coming from the coast and in particular from the Mediterranean waters intrusion (Konovalov et al., 2003).

The comparison of model results with physical (e.g. temperature, PAR profiles, mixing layer depth), chemical (e.g. nitrate, ammonium, silicate, oxygen, hydrogen sulfide) and biological (e.g.

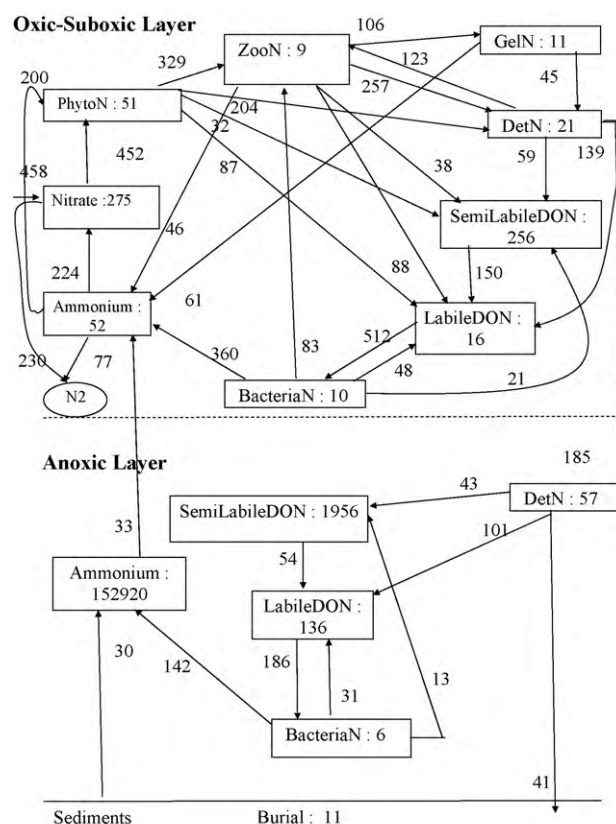


**Fig. 7.** The model-derived nitrogen budget (in  $\text{mmol N m}^{-2} \text{ year}^{-1}$ ). The Oxidic-Suboxic layer has been defined as the first upper 115 m (i.e. the layer where oxygen is present). The boxes represent model state variables. The vertically integrated content of each model state variable is indicated inside the boxes in  $\text{mmol N m}^{-2}$ .  $\text{N}_2$  is the end-product of denitrification (this is not a state variable, we put it for clarity of the scheme). All the model state variables of the upper and anoxic layer are connected by vertical transport processes. For clarity of the scheme, we only represent the vertical exchange of ammonium and PON because they are the only ones that have an order of magnitude comparable to the other biogeochemical flows.

chlorophyll, phytoplankton and mesozooplankton biomass, primary and bacterial production, export fluxes) data available in the Black Sea TU Ocean Base has shown a satisfactory good agreement and is described in Grégoire et al. (2008).

## 3.2. Budgets

### 3.2.1. Nitrogen and carbon budgets

The model-derived annual N- and C-budgets within the oxic-suboxic zone and the anoxic layer are presented respectively in Figs. 7 and 8.

In the upper layer, due to the small differences in standing stock of some constituents at the beginning and end of the integration period, the nitrogen budget appears slightly unbalanced, but total nitrogen is conserved. In the anoxic layer, the nitrogen budget is unbalanced: the source of nitrogen (i.e. the flux of PON sedimenting from the upper layer ecosystem) exceeds the loss (i.e. the upward flux of ammonium oxidized into  $\text{N}_2$  by the ANaerobic AMMONium OXidation (ANAMMOX) in the suboxic layer and the amount of nitrogen buried in the sediment). Also, we simulate an annual increase of the ammonium content of the deep waters of  $139 \text{ mmol N m}^{-2} \text{ year}^{-1}$ , corresponding to  $\approx 0.417 \times 10^{11} \text{ mol N year}^{-1}$  (considering that the horizontal surface of the deep sea is close to  $3 \times 10^{11} \text{ m}^2$ ) which is in perfect agreement with the predicted increase of  $0.42 \times 10^{11} \text{ mol year}^{-1}$  made by Konovalov and Murray (2001) from the analysis of in situ obser-

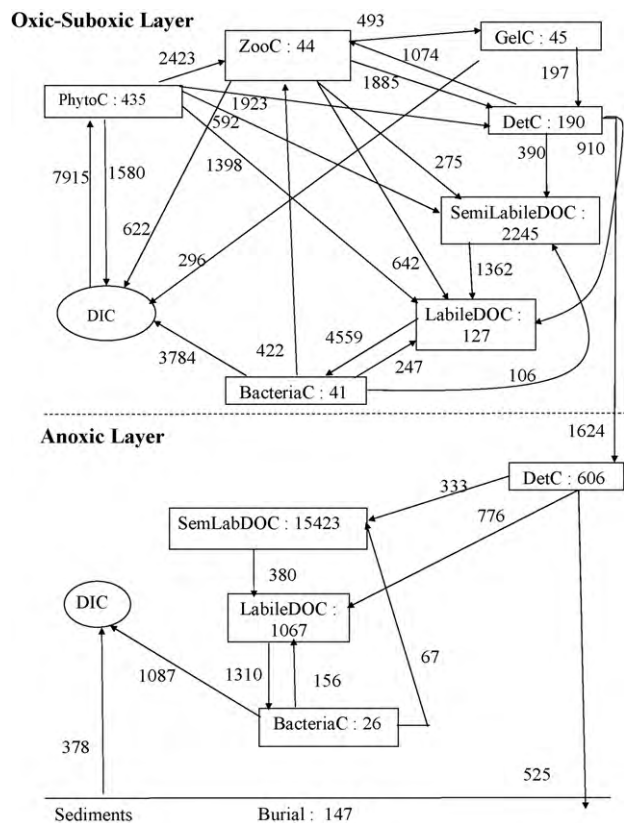


**Fig. 8.** The model-derived carbon budget (in  $\text{mmol C m}^{-2} \text{ year}^{-1}$ ). The Oxidic-Suboxic layer has been defined as the first upper 115 m (i.e. the layer where oxygen is present). The boxes represent model state variables. The vertically integrated content of each model state variable is indicated inside the boxes in  $\text{mmol C m}^{-2}$ . DIC is the end-product of respiration and is consumed by photosynthesis (this is not a state variable, we put it for clarity of the scheme). All the model state variables of the upper and anoxic layer are connected by vertical transport processes. For clarity of the scheme, we only represent the vertical exchange of POC because this is the only one that has an order of magnitude comparable to the other biogeochemical flows.

variations. This leads to an annual increase of the ammonium stock by 0.09%.

In the upper layer, an amount of  $652 \text{ mmol N m}^{-2}$  was converted each year from dissolved inorganic nitrogen to particulate form through phytoplankton assimilation. Compared with the upper layer total nitrogen load of  $701 \text{ mmol N m}^{-2}$ , this gives a turnover time of upper water column nitrogen of about one year (1.1 year). The nitrogen content of the living variables (i.e. phytoplankton, zooplankton and gelatinous) is at least one order of magnitude lower than the biogeochemical fluxes associated to them giving very rapid turnover rate. The magnitude and fate of phytoplankton production are shown in Table 1, and the characteristics of the microbial loop are shown in Table 2.

The uptake of DIC and inorganic nitrogen by phytoplankton is mostly partitioned to grazing (31% and 50% for C and N, respectively) and senescence mortality (37% and 47% for C and N, respectively), while a small fraction (13% and 2% for C and N, respectively) is lost by exudation (i.e. passive leakage and, for the carbon, extra-excretion) and 19% of the DIC uptake is lost through respiration (Table 1).

In order to illustrate the seasonal variability of the C:N ratio of phytoplankton, DOM and POM, Fig. 9 shows the C:N ratio of diatoms, the labile DOM and POM simulated by the model. At the beginning of the early spring bloom, the water column is replenished in nutrients and the phytoplankton growth is limited by the light availability. Algae take up carbon and nitrogen in a constant

**Table 1**

Magnitude and fate of the phytoplankton GPP, N uptake and zooplankton (excluding the gelatinous groups) grazing in nitrogen and carbon. Rates are averaged annual fluxes, vertically integrated over the upper 115 m, in  $\text{mmol C m}^{-2} \text{ year}^{-1}$  (upper part) and  $\text{mmol N m}^{-2} \text{ year}^{-1}$  (lower part).

Phytoplankton	Fluxes	Zooplankton	Fluxes
GPP	7915	CGrazing	3918
Respiration	1580	Respiration	622
DOC exudation	999	Messyfeeding to DOC	918
Grazing	2423	Grazing by gelatinous	493
Senescence mortality	2914	Senescence mortality	779
		Egestion	1106
Nuptake	652	NGrazing	534
DON exudation	13	Messyfeeding to DON	126
Grazing	329	Grazing by gelatinous	106
Senescence mortality	310	Senescence mortality	160
		Excretion	46
		Egestion	97

**Table 2**

Characteristics of the bacterial loop. Rates are averaged annual fluxes vertically integrated over the upper 115 m, in  $\text{mmol C m}^{-2} \text{ year}^{-1}$  (left) and  $\text{mmol N m}^{-2} \text{ year}^{-1}$  (right).

	Fluxes		Fluxes
DOC production	4566	DON production	512
By autotrophic processes	1993	By autotrophic processes	119
By heterotrophic processes	2573	By heterotrophic processes	394
DOC uptake	4559	DON uptake	512

ratio ( $\approx 5-6$ ) until the exhaustion of nutrients. There is no active DOC exudation by phytoplankton and  $\approx 2\%$  of the fixed C and N was released as DOM with a C:N ratio similar to that assimilated. The C:N ratio of the POM pool is low ( $\approx 7$ ). When nitrogen is exhausted (i.e. surface  $\text{NO}_3 = 1 \mu\text{M}$  at day 85 and  $0.1 \mu\text{M}$  around day 100), the model shows that phytoplankton enter in an unbalanced growth phase: carbon assimilation continues at a high rate, whereas nitrogen assimilation is strongly limited. The C:N ratio of diatoms (Fig. 9) increases until it reaches its maximum level of 20 as represented in the unbalanced model of Tett (1998). During this phase, the model simulates, in agreement with previous studies (e.g. Van den

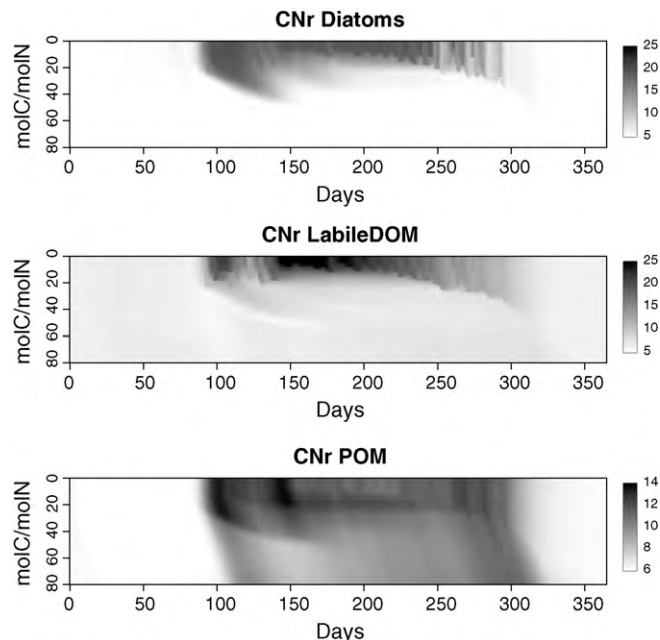


**Fig. 9.** Seasonal evolution of the vertical distribution of the C:N ratio (in  $\text{molC/molN}$ ) of diatoms (top), Labile DOM (middle) and POM (bottom) simulated by the model.

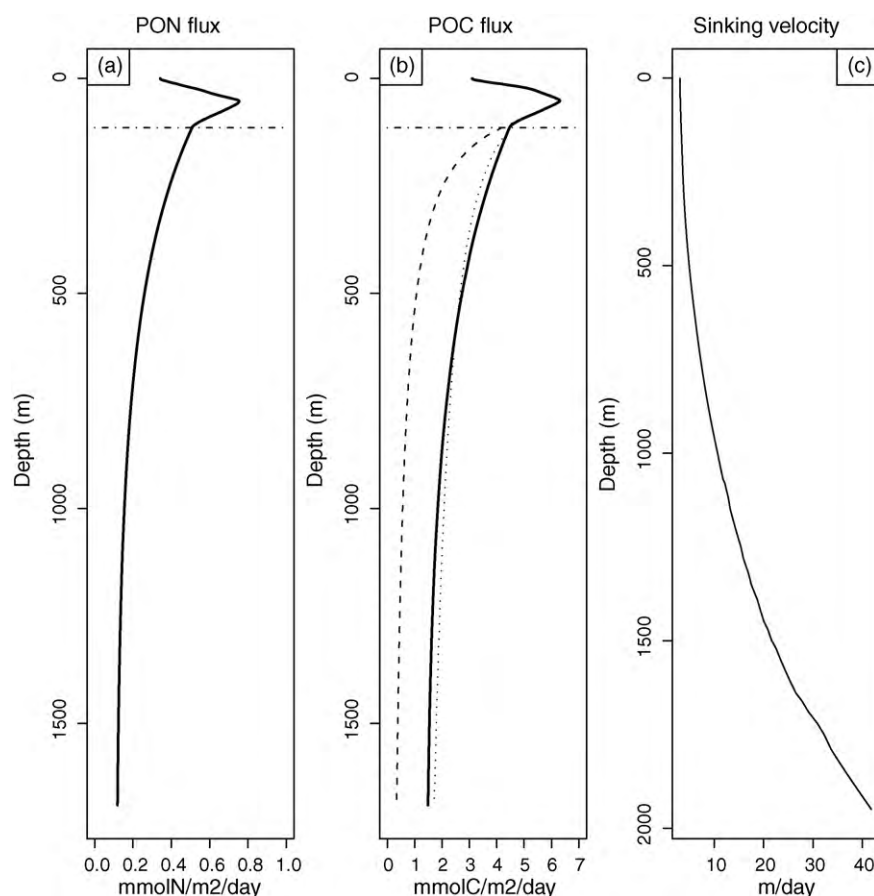


**Fig. 10.** Vertical annual mean profiles of the PON (a) and POC (b) fluxes (in respectively  $\text{mmolN m}^{-2} \text{day}^{-1}$  and  $\text{mmolC m}^{-2} \text{day}^{-1}$ ) and c) their sinking velocity (in  $\text{m day}^{-1}$ , computed from the aggregation model of Kriest (2002)). For the POC flux (b), bold: model results, dotted and dashed lines: profiles computed from equation  $C_R = C_{R,100m} (Z/100)^{-\alpha}$  established for the carbon rate by Martin et al. (1987) with respectively the attenuation coefficient  $\alpha = 0.85$  (averaged value for oxygenated oceanic areas) and  $\alpha = 0.36$  (value proposed by Devol and Hartnett, 2001 for anoxic environments). The dashed-dotted line represents the upper interface of the anoxic layer simulated at 115 m in the model.

Meersche et al., 2004), the accumulation of carbon-rich DOM with a C:N ratio of  $\approx 27$ –28 for the labile part (Fig. 9) and the production of POM with an increased C:N ratio of  $\approx 11$ –14 due to the intracellular increase in algal C:N ratio and the preferential degradation of PON compared to POC (see the values of parameters MaxHydPOC and MaxHydPON in Table A5). Over the year, the simulated algal carbon exudation is  $\approx 77$  times higher than the nitrogen exudation to overcome excess carbon assimilation in nutrients limited conditions. In the upper layer, heterotrophic mechanisms (e.g. dissolution of POM, zooplankton messy feeding, lysis of bacteria) contribute the most to the formation of DOM (56% and 77% for C and N, respectively) compared to autotrophic mechanisms (e.g. leakage, algal lysis, active exudation of carbon-rich DOM) (Table 2). According to our simulations, bacteria act throughout the year as ammonium remineralizers and never compete with algae for ammonium consumption. This means that, in the model, bacteria are able to consume the DOM without an additional source of nitrogen.

### 3.2.1.1. Primary and bacterial production, Community respiration.

The model-estimated annual averaged Gross Primary Production (GPP) is  $7.9 \text{ mol C m}^{-2} \text{ year}^{-1}$  or  $2.5 \times 10^{12} \text{ mol C year}^{-1}$  (Table 1). This value is in agreement with the values of  $2.8$ – $3.5 \times 10^{12} \text{ mol C year}^{-1}$  proposed by Stelmakh et al. (1998) and Vedernikov and Demidov (1997) for the primary production in the deep sea. The annual cycle of the simulated GPP presents a peak of  $0.14 \text{ mol C m}^{-2} \text{ day}^{-1}$  at the end of March and values between  $0.02$ – $0.035 \text{ mol C m}^{-2} \text{ day}^{-1}$  in May. These last values lie in the range of in situ estimations

made by Karl and Knauer (1991) in two stations in the central basin in May 1988 which were of  $0.027$  and  $0.047 \text{ mol C m}^{-2} \text{ day}^{-1}$ . The community respiration of the upper layer (CR defined as the total respiration of autotrophic and heterotrophic organisms) is estimated to  $6.3 \text{ mol C m}^{-2} \text{ year}^{-1}$ . This means that the upper layer ecosystem is net-autotrophic with a positive NCP (Net Community Production:  $\text{NCP} = \text{GPP} - \text{CR}$ ) of  $\approx 1.6 \text{ mol C m}^{-2} \text{ year}^{-1}$ . In the anoxic layer, bacterial respiration is estimated  $\approx 1.1 \text{ mol C m}^{-2} \text{ year}^{-1}$ .

The model-estimated annual averaged gross bacterial production in the upper layer is  $4.6 \text{ mol C m}^{-2} \text{ year}^{-1}$  (Table 2) with a peak of  $0.028 \text{ mol C m}^{-2} \text{ day}^{-1}$  at the end of March and values between  $0.02$  and  $0.026 \text{ mol C m}^{-2} \text{ day}^{-1}$  in May. These last values lie in the range of in situ estimations ( $0.021 \text{ mol C m}^{-2} \text{ day}^{-1}$ ) made by Karl and Knauer (1991) in two stations in the central basin in May 1988 during the KNORR expedition. Figures comparing the modeled GPP and bacterial production with observations are presented in Gregoire et al. (2008).

### 3.2.1.2. Denitrification.

The model estimates  $307 \text{ mmol N m}^{-2} \text{ year}^{-1}$  the annual amount of nitrogen definitely lost for the system in the form of nitrogen gas ( $\text{N}_2$ ). This means a basin wide loss of  $\approx 9 \times 10^{10} \text{ mol N year}^{-1}$ . The amount of nitrate lost represents  $230 \text{ mmol N m}^{-2} \text{ year}^{-1}$  (i.e.  $170 \text{ mmol N m}^{-2} \text{ year}^{-1}$  are used for the respiration of detritus,  $46 \text{ mmol N m}^{-2} \text{ year}^{-1}$  in the ANAMMOX reaction and  $14 \text{ mmol N m}^{-2} \text{ year}^{-1}$  for the oxidation of ODU). This value is almost twice higher than the value of  $\approx 125 \text{ mmol N m}^{-2} \text{ year}^{-1}$

**Table 3**  
Rates of some processes of the sulfide and carbon cycles in the anoxic layer. Data are from (1) Deuser (1971), (2) Karl and Knauer (1991), (3) Albert et al. (1995), (4) Muramoto et al. (1991), (5) Sorokin (1964), (6) Weber et al. (2001).

Processes	Observations mmol m <sup>-2</sup> year <sup>-1</sup>	Model output mmol m <sup>-2</sup> year <sup>-1</sup>
Carbon flux to the anoxic layer	1670 (1) 1190 (2) 1520 (3)	1624
Rate of sulfate reduction and sulfide production in the water column	79–536 (3)	535
Rate of sulfate reduction and sulfide production in sediment	144 (4) 470–530 (3) 290 (5) 219 (6)	188
Mean organic carbon flux to the sediments	389 (4)	525
Particulate sulfide flux	9.2 (4)	26
Rate of oxidation of sulfide at the top of interface	48 (4)	98

proposed by Konovalov et al. (2006). This difference is due to different estimations of the amount of nitrate used in the respiration of organic matter in oxygen deficient conditions. In the model, we simulate a vertically integrated annual consumption of 170 mmol N m<sup>-2</sup> while Konovalov et al. (2006) simulated very low values (almost zero). The amount of ammonium lost in the ANAMMOX reaction is estimated to 77 mmol N m<sup>-2</sup> year<sup>-1</sup> which is higher than the value of  $\approx 40$  mmol N m<sup>-2</sup> year<sup>-1</sup> proposed by Konovalov et al. (2006).

**3.2.1.3. Particle fluxes.** It has been found that in oxygen deficient environments, the degradation of POM is less efficient than in oxygenated water column (e.g. Harvey et al., 1995; Hedges et al., 1999; Devol and Hartnett, 2001). In the Black Sea, the lower efficiency of POM degradation in anoxic conditions was confirmed during the KNORR88 expedition. For instance, the study of the composition (e.g. the fatty acid signature, pigment composition) of the large sinking particles flux revealed a composition that remained almost unchanged when sinking through the anoxic water column (Wakeham and Beier, 1991; Repeta and Simpson, 1991). Also, in the model, in order to be able to simulate POM fluxes to the sediments in agreement with in situ data, we had to consider that POM decomposition in the anoxic water column is less efficient than in the oxygenated part. The degradation rate of POM depends on the oxygen concentration (for details refer to Grégoire et al., 2008). The simulated profiles of the annual mean vertical fluxes of POC and PON display a maximum at 40–50 m and below, the fluxes sharply decrease until the anoxic layer where they decrease much more slowly (Fig. 10a and b). This pattern is in agreement with sediment traps measurements performed during KNORR88 at two stations located in the central basin (Karl and Knauer, 1991). Indeed, these measurements revealed a rapid and efficient decomposition of the POM flux in the oxic-suboxic portion and low rates below. For instance, the POM flux decreases with a factor of 3–4 when sinking through the suboxic region and below that stayed relatively constant (Karl and Knauer, 1991).

Many sediments trap data performed in various marine environments suggest that the variation of the oceanic carbon rate with depth can be described using a power of function of depth:  $C_R = Z^{-\alpha}$  with  $\alpha$  being the attenuation coefficient. For instance, Martin et al. (1987) proposed the following formulation where the carbon rate has been normalized to the rain rate at 100 m ( $C_{R, 100m}$ ):  $C_R = C_{R, 100m} (Z/100)^{-\alpha}$ .

Published values for the attenuation coefficient  $\alpha$  from various well oxygenated oceanic areas range between 0.628 and 1.138, with the average being about 0.85 (Karl and Knauer, 1984; Martin et al., 1987; Bishop, 1989; Bender et al., 1992; Devol and Hartnett, 2001). In contrast, low attenuation rates of the carbon export were

found in oxygen deficient environments such as the Mexico margin ( $\alpha = 0.36$ , Devol and Hartnett (2001)), the coast of Peru (Martin et al., 1987) and the oxygen deficient zone of the Arabian Sea (Haake et al., 1992). The POC flux profile simulated by the model is presented in Fig. 10b and compared with other POC profiles reconstructed for oxic and anoxic environments. The simulated vertical POM profile in the Black Sea deep waters is very close to the curve obtained for other anoxic environments and using non-linear fitting technique, we also found a value of 0.36 for the attenuation coefficient  $\alpha$ .

As explained in Grégoire et al. (2008), the sinking speed of detritus is computed taking into account the possibility of aggregation of detritus following the model of Kriest (2002). We calibrated the stickness (i.e., the probability that two particles stick together after contact may vary from 0 to almost 1 parameter *stick*) in order to obtain a sinking speed vertical profile in agreement with the observations made by Asper (1988) on marine snow aggregates in the Black Sea. The model-simulated sinking velocity increases from a few m day<sup>-1</sup> in the upper 500 m to 40 m day<sup>-1</sup> in the bottom (Fig. 10c) which is in agreement with the range of 10–40 m day<sup>-1</sup> derived from observations (Asper, 1988).

**3.2.1.4. Particle fluxes to the anoxic layer.** According to Deuser (1971), the POC flux to the anoxic layer is 1.67 mol m<sup>-2</sup> year<sup>-1</sup>, of which 0.33 mol m<sup>-2</sup> year<sup>-1</sup> is buried as fossil carbon in the sediments. During the Black Sea KNORR cruise in May 1988, sediment traps deployed at two stations located in the central basin by Karl and Knauer (1991) yielded an annual value of 1.19 mol C m<sup>-2</sup> year<sup>-1</sup>, while sulphate rates reduction measurements in the water column and sediments by Albert et al. (1995) gave an annual POC flux of 1.52 mol m<sup>-2</sup> year<sup>-1</sup>. Also, the model simulated annual export of 1.6 mol C m<sup>-2</sup> year<sup>-1</sup> lies in the range of the integrated values derived from observations and corresponds to a total export of  $4.7 \times 10^{11}$  mol C year<sup>-1</sup>. The model estimates that  $\approx 20\%$  of the phytoplankton GPP is exported to the anoxic waters.

**3.2.1.5. Particle fluxes to the bottom.** Bottom sediment traps deployed at two sites (from October 1982 to May 1988) in the southwestern Black Sea and at one site in the central Black Sea (From 5 May to 13 July 1988) during the PARFLUX (Particle Flux Experiment) and during the 1988 R.V. Knorr expeditions (Hay et al., 1990; Muramoto et al., 1991) show that the seasonal variation of POC flux is very regular and predictable with roughly a two orders of magnitude difference between the low and high flux periods: high maximum fluxes and concentrations in the sediments occur in summer and autumn, 4–5 mmol C m<sup>-2</sup> day<sup>-1</sup>, and low fluxes occur in the winter and early spring, when fluxes are nearly zero, with an annual average flux of 0.39 mol C m<sup>-2</sup> year<sup>-1</sup>. In the model, the calibration of parameters *stick* and  $k_{sat, OxicHydro}$  associated respectively

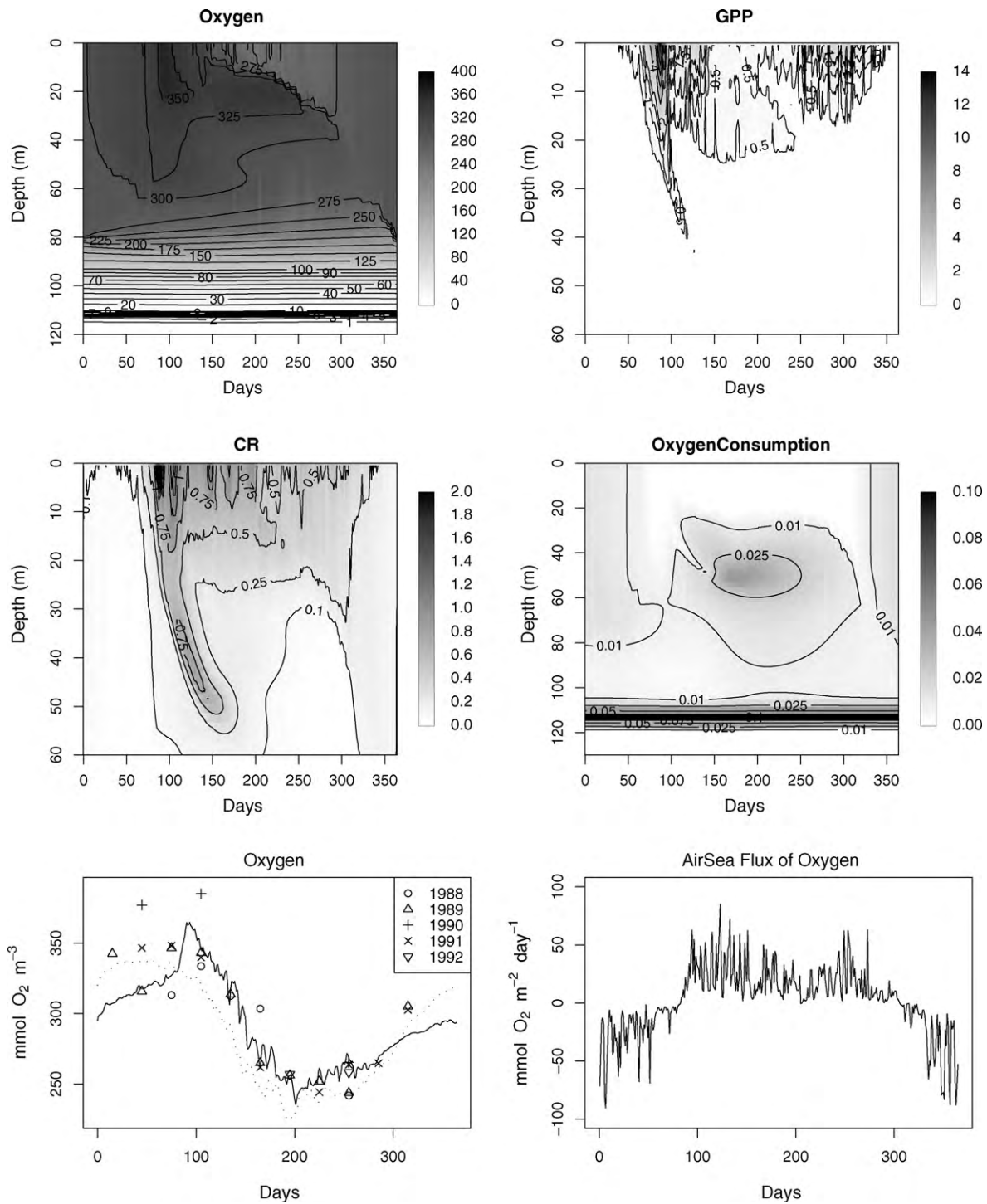


**Fig. 11.** Top and middle: Seasonal evolution of the vertical distribution of oxygen concentration (in mmol m<sup>-3</sup>), GPP (in mmol m<sup>-3</sup> day<sup>-1</sup>), CR (in mmol m<sup>-3</sup> day<sup>-1</sup>), oxygen consumption in nitrification and ODU oxidation (in mmol m<sup>-3</sup> day<sup>-1</sup>). Bottom: seasonal evolution of the surface oxygen concentration (in mmol m<sup>-3</sup>) simulated by the model (normal line) and from the data (symbols), the oxygen concentration in saturation (dotted line) and the air-sea exchange of oxygen (in mmol m<sup>-2</sup> day<sup>-1</sup>, positive values representing a flux from the sea to the atmosphere).

to the stickiness of aggregates and to the lower efficiency of POM degradation in anoxic conditions has allowed to produce integrated flux of POM to the sediments in agreement with in situ observations (see Table 3). The simulated annual averaged flux reaching the sediments is 0.52 mol C m<sup>-2</sup> year<sup>-1</sup> with a peak of 2 mmol C m<sup>-2</sup> day<sup>-1</sup> in spring and 10 mmol C m<sup>-2</sup> day<sup>-1</sup> in late summer. It should be noticed that if we used exactly the same decomposition rate of the POM in anoxic and oxic conditions (ignoring the lower effi-

ciency of POM degradation in anoxic conditions), particle fluxes to the bottom would have been strongly underestimated compared to sediment traps observations and the simulated hydrogen sulfide profiles would have been in disagreement with observations with too high concentrations in the water column.

Model results estimate that 33% of the amount of POC reaching the anoxic layer is degraded in the sediments. Active degradation in the sediments is confirmed by the high concentrations of dissolved

organic compounds (e.g. formate, acetate, glucose, fructose) and fluorescent compounds in the benthic boundary layer (Coble et al., 1991; Mopper and Kieber, 1991; Albert et al., 1995), as well as with the relationship established between organic carbon content and hydrogen sulfide in the sediment and sinking fluxes (more details in Muramoto et al. (1991)).

Burial seems to be enhanced in anoxic environment with a reported rate of 28% for the Black Sea and 30% for the Mexico margin (Devol and Hartnett, 2001).

### 3.2.2. Oxygen budget

**3.2.2.1. The seasonal cycling of oxygen.** The dynamics of oxygen in the surface layer is governed by the exchange with the atmosphere, vertical mixing, photosynthesis and respiration processes. The direction of the air-sea exchange of oxygen is determined by the sign of the difference between the surface oxygen concentration and the saturation concentration. The amount of oxygen that can be contained in the surface water at saturation depends on the temperature and salinity of the water. Since the surface salinity exhibits far smaller changes than temperature throughout the year at  $\approx 18.5$ , the seasonal evolution of the oxygen saturation concentration is governed by the evolution of water temperature (i.e. it exponentially decreases with temperature) reaching a minimum in summer and a maximum in February–March (Fig. 11). Therefore, surface waters are over-saturated in oxygen in summer and under-saturated in winter as shown by the direction of the air–sea flux (Fig. 11). We have an outgasing of oxygen to the atmosphere from early April until November. In winter, surface waters are enriched in oxygen from the atmosphere thanks to the vertical mixing. Surface oxygen concentrations reach 300–325  $\text{mmol m}^{-3}$  in January–February. Waters below 75–80 m are not ventilated and thus from this depth, the oxygen concentration sharply decreases and there is no more oxygen below 115 m. In early April, the surface oxygen concentration reaches a maximum of 368  $\text{mmol m}^{-3}$  because the GPP largely exceeds the CR (Fig. 11). At this period, water releases oxygen toward the atmosphere due to the increase of surface oxygen concentration thanks to an excess of GPP over CR and to the decrease of the saturation oxygen concentration with increasing surface temperature. This is at this period that the release of oxygen is at maximum. After the peak of GPP, the surface oxygen concentration decreases. From the end of May until end of July, GPP is lower than CR and the NCP is negative in the surface layer. In August and September, the NCP is positive in the surface layer and the surface oxygen concentration increases again. This is only in early November that surface waters are enriched in oxygen by the air–sea flux when the saturation concentration increases with decreasing temperature. The flux of oxygen is maximum at the end of December–early January.

The nitrification process reaches a peak in summer at 50 m when the regenerated ammonium accumulates. However, the maximum intensity of this process is  $\approx 0.05 \text{ mmol O}_2 \text{ m}^{-3} \text{ day}^{-1}$  and thus, this is half the value of CR at the same period and depth. Waters below  $\approx 80$  m are not ventilated, the oxygen concentration sharply decreases. In the layer 105–115 m oxygen is used to oxidize reduced compounds diffusing from the anoxic layer with a rate ranging from  $\approx 0.02$  to  $0.1 \text{ mmol O}_2 \text{ m}^{-3} \text{ day}^{-1}$ .

**3.2.2.2. The budget.** The oxygen dynamics is mainly governed by photosynthesis and respiration processes as well as by air–sea exchanges (Fig. 12).  $\approx 71\%$  of the oxygen produced by phytoplankton through photosynthesis and nitrate reduction (i.e. two moles of oxygen are released when phytoplankton consume one mole of nitrate) is lost by respiration,  $\approx 21\%$  by outgasing to the atmosphere,  $\approx 5\%$  through nitrification and only  $\approx 2\%$  in the oxidation of reduced components. These numbers are in perfect agreement with the findings of Yakushev et al. (2007) and Konovalov et al.

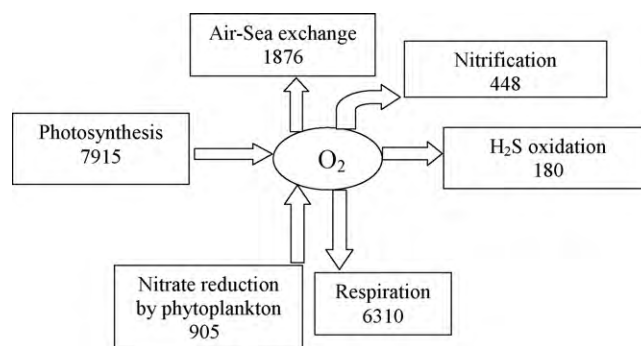


Fig. 12. The model-derived oxygen budget (in  $\text{mmol m}^{-2} \text{ year}^{-1}$ ) (vertically integrated values).

(2006) who found with their biogeochemical model that 70–78% of the oxygen produced by photosynthesis was lost by respiration while only 10–11% was lost through nitrification and only a few percents (4% for Konovalov et al., 2006) was lost by oxidation of reduced compounds other than ammonium. The model-estimated nitrification rate of  $448 \text{ mmol m}^{-2} \text{ year}^{-1}$  is in perfect agreement with the value of  $365 \text{ mmol m}^{-2} \text{ year}^{-1}$  proposed by Konovalov et al. (2006). The model estimates that the consumption of oxygen for oxidizing reduced compounds (other than ammonium) is very low compared to respiration and nitrification. According to Konovalov et al. (2006) and Konovalov et al. (2003), these reduced compounds are in fact oxidized by the oxygen brought in the Mediterranean plume. This lateral input is not represented in this study.

### 3.2.3. Sulfide budget

**3.2.3.1. Sulfide production.** Data collection on sulfate consumption, sediment trap observations and the analysis of the vertical profiles of particles composition have all shown that bottom sediments are essential places for sinking POM degradation while degradation in the 2000 m anoxic water column is not important except in the upper part (e.g. Muramoto et al., 1991; Albert et al., 1995). The model estimates that sulfide production in the sediments represents  $188 \text{ mmol m}^{-2} \text{ year}^{-1}$  while in the water column  $535 \text{ mmol m}^{-2} \text{ year}^{-1}$  are produced (see Table 3). It means that 26% of the sulfide production occurs in the sediment. This percentage is in agreement with the value of 18% found by Konovalov et al. (2006) with their chemical model. Sulfate reduction rates measured during the KNORR88 cruise have shown that the water column and sediments areal sulfate reduction rates on a depth integrated basis have comparable values, but on a volume basis the sediment rates are several thousand times higher than the water column rates (Albert et al., 1995). Also, the integration in time and depth of in situ measurements gives values in the range of model estimations with values of  $144\text{--}530 \text{ mmol m}^{-2} \text{ year}^{-1}$  for sulfide production in the sediments and of  $79\text{--}536 \text{ mmol m}^{-2} \text{ year}^{-1}$  for sulfide production in the water column (Table 3). Therefore, it is postulated that a non negligible fraction of the sulfide in the water column may be “old” sulfide upwelling and diffusing from below, rather than “new” sulfide produced from local sulfate reduction in the upper anoxic water column (Muramoto et al., 1991). Similar results have been found for the Cariaco Trench, where Scranton et al. (1987) have shown that the hydrogen sulfide in the water column can be attributed to upward diffusion from the bottom with water column production having little importance.

**3.2.3.2. Sulfide consumption: sulfide oxidation and metal sulfide precipitation.** The model estimates that  $98 \text{ mmol m}^{-2} \text{ year}^{-1}$  of reduced compounds (i.e. ODU, mainly of H<sub>2</sub>S) is oxidized annually. This means that only 13% of the produced sulfide is consumed by oxidation. This is due to the fact that the oxygen in the sub-

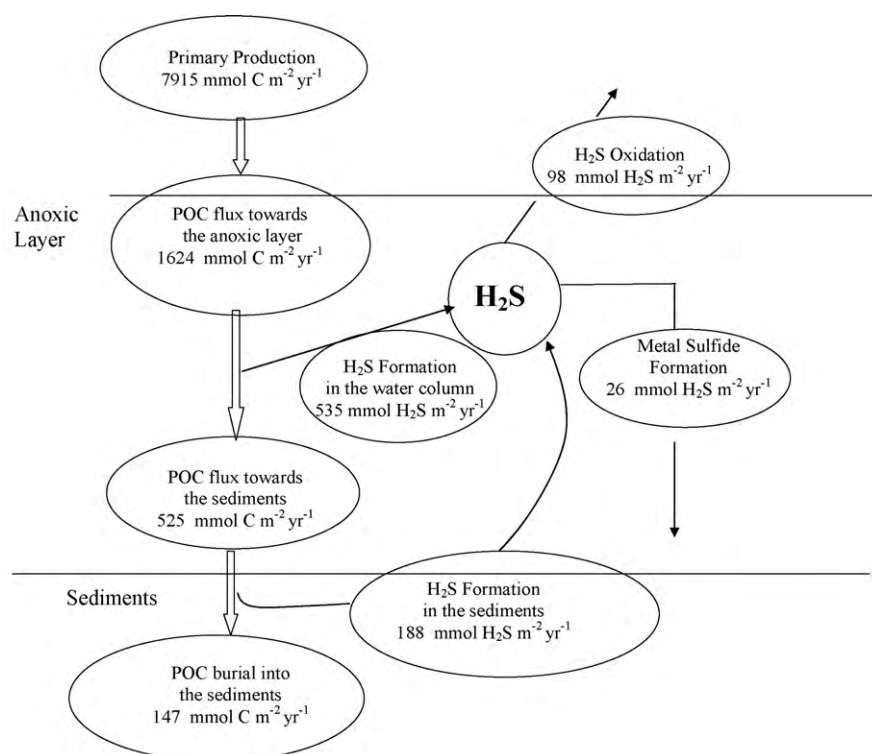


Fig. 13. The model-derived carbon and sulfide budgets (in  $\text{mmol m}^{-2} \text{ year}^{-1}$ ) for the deep anoxic layer.

oxic layer does not have concentrations high enough in order to lead to substantial oxidation of the hydrogen sulfide diffusing from the anoxic layer. In their paper, [Konovalov et al. \(2006\)](#) found that  $\approx 145 \text{ mmol m}^{-2} \text{ year}^{-1}$  of sulfide is oxidized in the water column while  $\approx 255 \text{ mmol m}^{-2} \text{ year}^{-1}$  is oxidized by the oxidants (mainly oxygen) present in the Bosphorus plume.

Metal sulfide precipitation occurs in the upper part of the anoxic layer where dissolved iron is available. Parameters  $R_{\text{solid}}$  and  $k_{\text{sat,iron}}^{\text{SolForm}}$  are calibrated in order to simulate a profile of  $\text{H}_2\text{S}$  in the upper part of the anoxic layer and a particulate sulfide production in agreement with observations. The simulated annual particulate sulfide flux of  $26 \text{ mmol m}^{-2} \text{ year}^{-1}$  is by three times higher than the in situ measured value of  $9.2 \text{ mmol m}^{-2} \text{ year}^{-1}$  given by [Muramoto et al. \(1991\)](#) (Table 3).

The overestimation by the model of particulate sulfide formation and sulfide oxidation which are both the main processes of sulfide consumption in the upper part of the anoxic layer, is necessary in order to simulate  $\text{H}_2\text{S}$  concentrations in this region in agreement with observations. This problem can be partly explained by the absence, in this 1D model, of lateral injection of oxygen from coastal areas and also from the Bosphorus area. [Albert et al. \(1995\)](#) and [Konovalov et al. \(2003\)](#) have estimated that the oxygen brought by Mediterranean waters could be responsible for the oxidation of  $\approx 255\text{--}370 \text{ mmol H}_2\text{S m}^{-2} \text{ year}^{-1}$  (about half of the model-estimated annual sulfide production of  $723 \text{ mmol m}^{-2} \text{ year}^{-1}$ ). However, it should be noted that this oxidation process is a localized effect and mainly concerns the Bosphorus area.

**3.2.3.3. The budget.** As for nitrogen in the anoxic layer, the sulfide budget is unbalanced: the annual sulfide production associated to the anoxic degradation of the sinking POM exceeds sulfide consumption by oxidation and particulate sulfide formation. Also, we simulate an annual increase of the sulfide content of the deep waters of  $599 \text{ mmol m}^{-2} \text{ year}^{-1}$ , corresponding to  $\approx 1.8 \times 10^{11} \text{ mol year}^{-1}$ . If we consider

that an additional amount of  $\approx 255\text{--}370 \text{ mmol m}^{-2} \text{ year}^{-1}$  of sulfide can be oxidized by the Bosphorus plume, we still have an unbalanced budget with an increase of  $\approx 230\text{--}345 \text{ mmol m}^{-2} \text{ year}^{-1}$ .

The simulated increase of hydrogen sulfide is not uniform over the whole anoxic layer: it is more important above the sediments where a huge part of the POM is degraded. Also, the  $\text{H}_2\text{S}$  concentration increases by  $0.5 \text{ mmol m}^{-3} \text{ year}^{-1}$  at 180 m and by  $1.3 \text{ mmol m}^{-3} \text{ year}^{-1}$  at 2000 m. The increase is less marked in the middle of the anoxic zone (e.g.  $0.25 \text{ mmol m}^{-3} \text{ year}^{-1}$  at 800 m) due to the reduced remineralization at these depths compared to sediments and the upper part of the anoxic zone (the sinking velocity is much higher at 1000 m than at 150 m, see Fig. 10) and the very low vertical mixing (mainly associated with molecular diffusion) that is unable to transport rapidly the sulfide produced in the sediments and upper anoxic layer to intermediate depths. These findings are in agreement with the analysis of in situ observations performed by [Konovalov and Murray \(2001\)](#) that reveals consistent temporal variations in the concentration of sulfide within the anoxic zone at different depths and density surfaces with a continual increase at a given depth ranging from  $0.8$  to  $2.2 \mu\text{M year}^{-1}$  since 1985. As in the model, this increase is more rapid and significant in the deep layers than in the upper part of the sulfidic layer (see Fig. 7, [Konovalov and Murray, 2001](#); Fig. 13).

#### 4. Conclusion

Carbon, nitrogen, oxygen and sulfide flows through the whole Black Sea water column have been quantified using a coupled physical–biogeochemical model. The model involves a refined representation of the foodchain from bacteria to gelatinous carnivores. It includes a description of particular processes occurring in oxygen deficient environments such as the degradation of organic matter using different types of oxidants, ANAMMOX and specific redox reactions. The model is run in the deep sea (depth  $\approx 2000$  m) with

nitrate and silicate concentrations typical of the eutrophication period (i.e. end of the 1980s).

The carbon and nitrogen cycling derived for the upper layer shows that the flows between biogeochemical compartments are by  $\approx$  one order of magnitude higher than the integrated carbon and nitrogen content of the different compartments (except for the semi-labile DOM). This gives a turnover time for the upper water column nitrogen of the order of the year. The model simulates an important variation of the C:N ratio of phytoplankton, POM and DOM increasing substantially at the end of the bloom when nutrients are exhausted. Indeed, starting from almost Redfield values of  $\approx$ 5–7, this ratio reaches values of 20, 27–28 and 11–14 for respectively phytoplankton, DOM (labile part) and POM. In the upper layer, heterotrophic mechanisms (e.g. dissolution of POM, zooplankton messy feeding, lysis of bacteria) contribute the most to the formation of DOM (56% and 77% for C and N, respectively) compared to autotrophic mechanisms (e.g. leakage, algal lysis, active exudation of carbon-rich DOM).

The model-estimated annual averaged GPP is  $7.9 \text{ mol C m}^{-2} \text{ year}^{-1}$  of which 20% ( $1.6 \text{ mol C m}^{-2} \text{ year}^{-1}$ ) reaches the anoxic layer and is definitely lost for the upper layer ecosystem. For the upper layer, the model estimates a CR of  $6.3 \text{ mol C m}^{-2} \text{ year}^{-1}$  and thus a NCP equals to the export of  $1.6 \text{ mol C m}^{-2} \text{ year}^{-1}$ . The system is thus net-autotrophic.

The oxygen dynamics is mainly governed by photosynthesis and respiration processes as well as by air–sea exchanges.  $\approx$ 71% of the oxygen produced by phytoplankton (photosynthesis+nitrate reduction) is lost through respiration,  $\approx$ 21% by outgassing to the atmosphere,  $\approx$ 5% through nitrification and only  $\approx$ 2% in the oxidation of reduced components.

The model estimates  $307 \text{ mmol N m}^{-2} \text{ year}^{-1}$  the amount of nitrogen lost through denitrification. This gives a basin wide loss of  $\approx 9 \times 10^{10} \text{ mol N year}^{-1}$ .  $\approx$ 55% is lost through the use of nitrate for the oxidation of detritus in low oxygen conditions,  $\approx$ 40% in the ANAMMOX reaction and the remaining  $\approx$ 5% in the oxidation of reduced substances by nitrate.

The model estimated amount of POC reaching the bottom and the sulfide produced in the water column and in the sediments are in the range of available observations. This good agreement requires to use a formulation of the POM degradation depending on the oxygen content and to compute the sinking speed based on an aggregation model. Moreover, the obtained profile of the vertical flux of POC is in perfect agreement with the mathematical formulation proposed by Devol and Hartnett (2001) for anaerobic environments. 33% ( $0.52 \text{ mol C m}^{-2} \text{ year}^{-1}$ ) of the organic matter sinking to the anoxic layer reaches the sediments for being degraded. In the anoxic water column, POM degradation mainly occurs in the upper part of the anoxic layer because the sinking speed of settling POM rapidly increases with depth due to particles aggregation.

The sulfide and nitrogen budgets established for the anoxic layer are not balanced in response to the enhanced particle fluxes induced by eutrophication: the  $\text{NH}_4$  and  $\text{H}_2\text{S}$  concentrations increase. This increase is in agreement with data analysis performed on long time series collected since the 1960s (Kononov and Murray, 2001). The tendency is particularly noticeable in sites of active detritus degradation: in the sediments and in the upper part of the anoxic layer. It should be noted that this tendency may have been overestimated in the model due to the absence of lateral oxygen injections.

## Acknowledgments

This research was supported by the EU Marie Curie individual fellowship (contract no. HPMF-CT-2002-01562), the EU Marie Curie

reintegration grant (contract no. MERG-CT-2004-012756) and the EU SESAME project (contract no. GOCE-036949). Marilaure Grégoire is Research Associate at the Belgian Foundation for Scientific Research (FNRS). The numerical code of the physical model has been obtained from the GOTM web site (<http://www.gotm.net>). The ECMWF ERA-40 data used in this study have been obtained from the ECMWF data server (<http://www.ecmwf.net>). Biogeochemical data were provided by the Black Sea TU Ocean Base gathering data collected in the frame of NATO projects on the Black Sea (<http://sfp1.ims.metu.edu.tr/TU-BlackSea/>). This is the MARE publication no. 192 and the NIOO publication no. 4794.

## Appendix A. Supplementary data

Supplementary data associated with this article can be found, in the online version, at doi:10.1016/j.ecolmodel.2010.06.007.

## References

- Albert, D., Taylor, C., Martens, C., 1995. Sulfate reduction rates and low molecular weight fatty acid concentrations in the water column and surficial sediments of the black sea. *Deep Sea Research* 42, 1239–1260.
- Asper, V., 1988. Distribution of marine snow aggregates in the black sea and comparison with water column structure and suspended fine particle concentrations. *Eos* 69, 1240.
- Bender, M., Ducklow, H., Kiddon, J., Marra, J., Martin, J., 1992. The carbon balance during the 1989 spring bloom in the north atlantic ocean, 47°N, 20°W. *Deep Sea Research* 39, 1707–1726.
- Bishop, J., 1989. Regional extremes in particulate matter composition and flux: effects on the chemistry of the ocean interior. In: Berger, W., Smetacck, V., Wefer, G. (Eds.), *Productivity of the Ocean: Present and Past*.
- Blackford, C., Allen, J., Allen, F., 2004. Ecosystem dynamics at six contrasting sites: a generic modelling study. *Journal of Marine Systems* 52, 191–215.
- Buesseler, K., Livingston, H., Ivanov, L., Romanov, A., 1991. Stability of the oxic/anoxic interface in the black sea. *Deep Sea Research* 41, 283–296.
- Coble, P., Gagosian, R., Codispoti, L., Friederich, G., Christensen, J., 1991. Vertical distribution of dissolved and particulate fluorescence in the black sea. *Deep Sea Research II* 38 (Suppl. 2A), 985–1002.
- Cociasu, A., Diaconu, V., Popa, L., Buga, L., Nae, I., Doragan, L., Malciu, V., 1997. The Nutrient Stock of the Romanian Shelf of the Black Sea During the Last Three Decades. Kluwer Academic Publishers, Dordrecht.
- Codispoti, L., Friederich, G.E., Murray, J., Sakamoto, C., 1991. Chemical variability in the black sea: implications of continuous vertical profiles that penetrated the oxic/anoxic interface. *Deep Sea Research II* 38 (Suppl. 2A), 691–710.
- Deuser, W., 1971. Organic carbon budget of the black sea. *Deep Sea Research* 18, 995–1004.
- Devol, A., Hartnett, H., 2001. Role of the oxygen deficient zone in transfer of organic carbon to the deep ocean. *Limnology and Oceanography* 46, 1684–1690.
- Grégoire, M., Raïck, C., Soetaert, K., 2008. Numerical modeling of the deep black sea ecosystem functioning during the late 1980s (eutrophication phase). *Progress in Oceanography* 76, 286–333.
- Grégoire, M., Friedrich, J., 2004. Nitrogen budget of the north-western black sea shelf as inferred from modeling studies and in-situ benthic measurements. *Marine Ecology Progress Series* 270, 15–39.
- Grégoire, M., Lacroix, G., 2003. Exchange processes and nitrogen cycling on the shelf and continental slope of the black sea basin. *Global Biogeochemical Cycles* 17, 42–I–42–17.
- Grégoire, M., Nezhin, N., Kostianoy, A., Soetaert, K., 2004. Modeling the nitrogen cycling and plankton productivity in an enclosed environment (the black sea) using a three-dimensional coupled hydrodynamical-ecosystem model. *Journal of Geophysical Research*, 109.
- Haake, B., Ittekkot, V., Ramaswamy, V., Nair, R., Honjo, S., 1992. Fluxes of amino acids and hexosamines to the deep arabian sea. *Marine Chemistry* 40, 291–314.
- Harvey, H., Tuttle, J., Bell, J., 1995. Kinetics of phytoplankton decay during simulated sedimentation: changes in biochemical composition and microbial activity under oxic and anoxic conditions. *Geochimica et Cosmochimica Acta* 59, 3367–3377.
- Hay, B., Honjo, S., Kempe, S., Ittekkot, V., Degens, E., Konuk, T., Izdar, E., 1990. Interannual variability in particle flux in the southwestern black sea. *Deep Sea Research* 37, 911–928.
- Hedges, J., Hu, F., Devol, A., Hartnett, H., Tsamakias, E., Keil, R., 1999. Sedimentary organic matter preservation: a test for selective degradation under oxic conditions. *American Journal of Science* 299, 529–555.
- Humborg, C., Ittekkot, V., Cociasu, A., Bodungen, B., 1997. Effect of danube river dam on black sea biogeochemistry. *Nature* 386, 385–388.
- Karl, D., Knauer, G., 1991. Microbial production and particle flux in the upper 350 m of the black sea. *Deep Sea Research II* 38 (Suppl. 2A), 921–942.
- Karl, D., Knauer, K., 1984. Vertical distribution, transport and exchange of carbon in the northeast pacific ocean: evidence for multiple zones of biological activity. *Deep Sea Research* 31, 245–270.

- Kideys, A., Kovalev, A., Shulman, G., Gordina, A., Bingel, F., 2000. A review of zooplankton investigations of the black sea over the last decade. *Journal of Marine Systems* 24, 355–371.
- Konovalov, S., Luther, G., Friederich, G., Nuzzio, D., Tebo, B., Murray, J., Oguz, T., Glaze, B., Trouwborst, R., Clement, B., Murray, K., Romanov, A., 2003. Lateral injection of oxygen with the bosphorus plume-fingers of oxidizing potential in the black sea. *Limnology and Oceanography* 48 (6), 2369–2376.
- Konovalov, S., Murray, J., 1960–1995. Variations in the chemistry of the black sea on a time scale of decades. *Journal of Marine Systems* 31, 217–243.
- Konovalov, S., Murray, J., Luther, G., Tebo, B., 2006. Processes controlling the redox budget for the oxic/anoxic water column of the black sea. *Deep Sea Research II* 53, 1817–1841.
- Kovalev, A., Piontkovski, S., 1998. Interannual changes in the biomass of the black sea gelatinous zooplankton. *Journal of Plankton Research* 20 (7), 1377–1385.
- Kriest, I., 2002. Different parameterizations of marine snow in a 1D-model and their influence on representation of marine snow, nitrogen budget and sedimentation. *Deep Sea Research I* 49, 2133–2162.
- Lancelot, C., Staneva, J., Van Eeckhout, D., Beckers, J., Stanev, E., 2002. Modelling the danube-influenced north-western continental shelf of the black sea. II: Ecosystem response to changes in nutrient delivery by danube river after its damming in 1972. *Estuarine, Coastal and Shelf Science* 54, 473–499.
- Lebedeva, L., Shushkina, E., 1994. The model investigation of the black sea community changes caused by menmiosis. *Oceanology* 34, 79–87.
- Martin, J., Knauer, K., Karl, D., Broenkow, W., 1987. Vertex: carbon cycling in the northeast pacific. *Deep Sea Research* 34, 267–285.
- Mee, L., 1992. The black sea in crisis: the need for concerted international action. *Ambio* 21, 278–286.
- Mikaelyan, A., 1997. Long-Term Variability of Phytoplankton Communities in Open Black Sea in Relation to Environmental Changes. Kluwer Academic Publishers, Dordrecht.
- Mopper, K., Kieber, D., 1991. Distribution and biological turnover of dissolved organic compounds in the water column of the black sea. *Deep Sea Research II* 38 (Suppl. 2A), 1021–1048.
- Muramoto, J., Honjo, S., Fry, B., Hay, B., Howarth, R., Cisne, J., 1991. Sulfur, iron and organic carbon fluxes in the black sea: sulfur isotopic evidence for origin of sulfur fluxes. *Deep Sea Research II* 38 (Suppl. 2A), 1151–1188.
- Murray, J., Codispoti, L., Friederich, G., 1995. Redox environments: the suboxic zone in the black sea. In: Huang C., Melia C., Morgan J. (Eds.), *Aquatic Chemistry: Interfacial and Interspecies Processes*. pp. 157–176.
- Murray, J., Jannasch, H., Honjo, S., Anderson, R., Reeburgh, W., Top, Z., Friederich, G., Codispoti, L., Izdar, E., 1989. Unexpected changes in the oxic/anoxic interface in the black sea. *Nature* 338, 411–413.
- Murray, J., the Black Sea Knorr Expedition, 1991. Black sea oceanography. Results from the 1988 black sea expedition. *Deep Sea Research II* 38 (Suppl. 2A), 1266.
- Murray, J., Top, Z., Ozsoy, E., 1991. Hydrographic properties and ventilation of the black sea. *Deep Sea Research II* 38 (Suppl. 2A), 663–689.
- Niermann, U., Bingel, F., Gorban, A., Gordina, A., Gücü, A., Kideys, E., Konsulov, A., Radu, G., Subbotin, A., Zaika, V., 1994. Distribution of anchovy eggs and larvae (*engraulis encrasicolus* cuv.) in the black sea in 1991–1992. *ICES Journal of Marine Science* 51, 395–406.
- Oguz, T., Ducklow, H., Malanotted-Rissoli, P., Tugrul, S., Nezlín, N., Unluata, U., 1996. Simulation of the annual plankton productivity cycle in the black sea by a one-dimensional physical-biological model. *Journal of Geophysical Research* 101 (C7), 16585–16599.
- Oguz, T., Ducklow, J., Malanotte-Rizzoli, P., 2000. Modeling distinct vertical biogeochemical structure of the black sea: dynamical coupling of the oxic, suboxic, and anoxic layers. *Global Biogeochemical Cycles* 14 (4), 1331–1352.
- Oguz, T., Ducklow, J., Purcell, J., Malanotte-Rizzoli, P., 2001. Modeling the response of top-down control exerted by gelatinous carnivores on the black sea pelagic food web. *Journal of Geophysical Research* 106 (C3), 4543–4564.
- Ozsoy, E., Unluata, U., 1997. Oceanography of the black sea: a review of some recent results. *Earth Science Reviews* 42 (4), 231–272.
- Repeta, D., Simpson, D., 1991. The distribution and recycling of chlorophyll, bacteriochlorophyll and carotenoids in the black sea. *Deep Sea Research II* 38 (Suppl. 2A), 969–984.
- Saydam, S., Tugrul, S., Basturk, O., Oguz, T., 1993. Identification of the oxic/anoxic interface by isopycnal surfaces in the black sea. *Deep Sea Research* 40, 1405–1412.
- Scranton, M., Sayles, F., Bacon, M., Brewer, P., 1987. Temporal changes in the hydrography and chemistry of the cariacio trench. *Deep Sea Research* 34, 945–963.
- Shushkina, E., Vinogradov, M., 1991. Long term changes in the biomass of plankton in open areas of the black sea. *Marine Biology* 89, 95–107.
- Sorokin, Y., 1964. On the primary production and bacterial activities in the black sea. *Journal du Conseil Permanent International pour l'exploration de la Mer* 29, 41–60.
- Stanev, E., 1990. On the mechanisms of the Black Sea circulation. *Earth Science Reviews* 28, 285–319.
- Staneva, J., Stanev, E., Oguz, T., 1998. On the sensitivity of the planktonic cycle to physical forcing. Model study on the time variability of the black sea ecological system. In: Ivanov, L., Oguz, T. (Eds.), *Ecosystem Modeling as a Management Tool for the Black Sea*, vol. 2. NATO Sci. Partnership Sub-ser. 2, vol. 47, pp. 301–322.
- Stelmakh, L., Yunev, O., Finenko, Z.Z., Vedernikov, V.I., Bologa, A., Churilova, T.Y., 1998. Peculiarities of seasonal variability of primary production in the black sea. In: Ivanov, L., Oguz, T. (Eds.), *NATO TU-Black Sea Project Ecosystem Modeling as a Management Tool for the Black Sea, Symposium on Scientific Results*. NATO ASI Series 2/47 (1), 93–104.
- Tett, P., 1998. Parameterising a Microplankton Model. Napier University.
- Top, Z., Ostlund, O., Pope, L., Grall, C., 1991. Helium isotopes, neon and tritium in the black sea: a comparison with the 1975 observations. *Deep Sea Research II* 38 (Suppl. 2A), 747–760.
- Torres, R., Allen, J., Figueiras, F., 2006. Sequential data assimilation in an upwelling influenced estuary. *Journal of Marine Systems* 60, 317–329.
- Tugrul, S., Basturk, O., Saydam, C., Yilmaz, A., 1992. Changes in the hydrochemistry of the black sea inferred from water density profiles. *Nature* 352, 137–139.
- Unluata, U., Oguz, T., Latif, M., Ozsoy, E., 1990. On the physical oceanography of the turkish straits. In: Tratt, L.J. (Ed.), *The physical Oceanography of Sea Straits*. pp. 25–60.
- Van den Meersche, K., Middelburg, J., Soetaert, K., van Rijswijk, P., Boschker, H., Heip, C., 2004. Carbon-nitrogen coupling and algal-bacterial interactions during an experimental bloom: modeling a <sup>13</sup>C tracer experiment. *Limnology and Oceanography* 49 (3), 862–878.
- Vedernikov, V.I., Demidov, A.B., 1997. The vertical distribution of primary production and chlorophyll in the deep part of the black sea for different seasons. *Oceanology* 37 (3), 414–423.
- Wakeham, S., Beier, J., 1991. Fatty acid and sterol biomarkers as indicators of particulate matter source and alteration processes in the black sea. *Deep Sea Research II* 38 (Suppl. 2A), 943–968.
- Weber, A., Riess, W., Wenzhoefer, F., Jorgensen, B., 2001. Sulfate reduction in black sea sediments: in situ and laboratory radiotracer measurements from the shelf to 2000 m depth. *Deep Sea Research I* 48, 2073–2096.
- Yakushev, E., Neretin, L., 1997. One dimensional modeling of nitrogen and sulfur cycles in the aphotic zone of the black and arabian seas. *Global Biogeochemical Cycles* 11 (3), 401–414.
- Yakushev, E., Pollehne, F., Jost, G., Kuznetsov, I., Schneider, B., Umlauf, L., 2007. Analysis of the water column oxic/anoxic interface in the black and baltic seas with a numerical model. *Marine Chemistry* 107, 388–410.
- Yunev, O., Moncheva, S., Carstensen, J., 2005. Long-term variability of vertical chlorophyll a and nitrate profiles in the open black sea: eutrophication and climate change. *Marine Ecology Progress Series* 294, 95–107.
- Yunev, O., Verdernikov, V., Basturk, O., Yilmaz, A., Kideys, A., Moncheva, S., Konovalov, S., 2002. Long-term variations of surface chlorophyll a and primary production in the open black sea. *Marine Ecology Progress Series* 230, 11–28.